Chapter 7
Imaging with the Helium Ion Microscope

John Notte and Bernhard Goetze

Abstract A newly developed technology, the helium ion microscope (HIM), provides high-resolution imaging with several benefits compared to the standard scanning electron microscope (SEM). First, the images provide high resolution because the helium beam can be brought to a focused probe size that can be as small as 0.25 nm. Second, the images provide contrast mechanisms that are often markedly different from the SEM. These contrast mechanisms can reveal topographic, composition, and other types of information about the sample. Third, compared to the SEM, the HIM images tend to be more surface-specific – revealing information about the surface without the confusing subsurface information. Fourth, the HIM can obtain high-resolution images even of insulating samples that would otherwise charge excessively in the SEM. The HIM is still in its infancy compared to the SEM, having only been commercially available for 7 years; however, it has already provided several unique advantages for the imaging of biological materials.

7.1 Introduction: On the Importance of Surfaces

In many imaging and analysis applications, surface specificity is crucial to produce an easily interpreted image or data set. In fact, the nature of the human retina (essentially a 2D sensor) limits our eyes to gathering 2D information. Also, for uncounted years, our brains have been optimized for interpreting this 2D information as surface-specific information. The mixing of deeper information with the surface information tends to make the images harder to understand or downright deceptive (think smoke and fog). In a mathematical sense, the determination of 3D information from a 2D data set is a noninvertible problem. In other words, a single image does not

J. Notte (✉) • B. Goetze
Director of Research and Development, Carl Zeiss Microscopy,
Peabody, MA, USA
e-mail: john.notte@zeiss.com

V.S. Smentkowski (ed.), *Surface Analysis and Techniques in Biology*,
DOI 10.1007/978-3-319-01360-2_7,

provide enough information to unambiguously reveal both surface information and the deeper information. Hence, an imaging technique that provides surface-specific information offers a less ambiguous interpretation.

In many applications, surface specificity is of primary importance because the interface itself is the subject of the investigation. To a large extent, this is because the interfaces define the boundary between objects, and it is through these interfaces that objects can interact. Challenging applications of this nature occur in biology (e.g., cell membranes), semiconductor physics (e.g., doped silicon junctions), and material science (e.g., catalysis and corrosion). In most of these applications, the surfaces are critical because the most interesting chemical processes are limited to interfaces between different domains.

Many of the well-established high-resolution imaging techniques provide an ambiguous image that mixes the surface information with the deeper information. The well-established techniques of transmission electron microscope (TEM) and scanning transmission electron microscope (STEM) provide excellent resolution only after preparation of a ~100 nm thick lamella through which the beam passes. The lamella preparation can be time-consuming and there is a risk of damaging the specimen in the process. Because the beam passes through the lamella, the contrast in the image represents an average along the beam path through the sample rather than the true surface information. In addition, while the atomic force microscope (AFM) provides high-resolution surface analysis, it is limited to the subset of samples that can be directly contacted and have a very limited topography – a very small subset of biological specimens. The most routinely used high-resolution imaging instrument for biological samples is the scanning electron microscope (SEM). The images it provides are high-resolution and do provide a good image contrast that reveals different properties of the specimen. However, the SEM is known to produce much of its signal from the reemergence of backscatter electrons, which reveal "SE2" information about deeper layers – a topic of discussion in later sections here. This effect can be mitigated by operating the electron beam at lower energies, but this tends to limit the lateral resolution by chromatic aberration effects. The operation of the SEM also induces charging on and under the surface of the sample – effects that can compromise the image quality and can even damage the specimen. Metal coatings are sometimes used to improve the charging and surface specificity of the SEM, but the coatings often obscure the fine-scale features of interest and even also damage the sample. Operating the SEM in the presence of gases (such as water or nitrogen) can help to mitigate the surface-charging effects, but subsurface charging is not resolved, and the gases tend to limit the resolution.

In contrast, the newly developed technology of the helium ion microscope (HIM) produces high-resolution images with *inherent* surface specificity. The surface-specific nature of the images is a direct consequence of the physics of the helium ion as it interacts with the specimen. The charging effects are also fundamentally different from the SEM and are much more readily mitigated. Figure 7.1 is an HIM image of the iron oxidizing Acidovorax Proteobacteria (strain BoFeN1). This sample was originally isolated from the anoxic freshwater sediments of Lake Constance in Germany and was provided by Martin Obst and Fabian Zeitvogel, University of

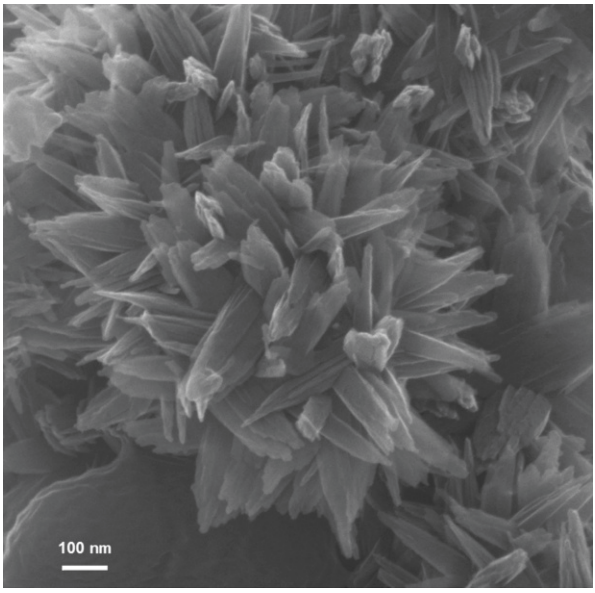

Fig. 7.1 A high-magnification helium ion microscope image of Acidovorax (Sample provided by Martin Obst and Fabian Zeitvogel of the University of Tuebingen)

Tuebingen, Germany. When grown in the presence of Fe(II), some cells tend to form a crust of Fe(III) mineral needles. Imaging with an HIM reveals the structure of those mineral crusts on the cell surface for the first time. Imaging in the SEM requires platinum coatings, which incidentally adulterate the real structure and introduce artifacts [1].

In this chapter, the basic technology of the HIM is first explained. Subsequently, the unique interaction of the beam with the sample is described in detail for a range of beam energies and samples. Specifically addressed are the image formation process and the properties of the sample, which are revealed in the resulting image. The unique charging advantages and the minimal sample preparation requirements are then described in detail. Lastly, the future outlook of this technology is provided.

7.2 Technology of the Helium Ion Microscope

7.2.1 Overview

Much of the technology discussed here is contained within the Zeiss family of helium ion microscopes: the ORION Plus™ and the ORION NanoFab™. These models have only recently become commercially available [2] after many years of

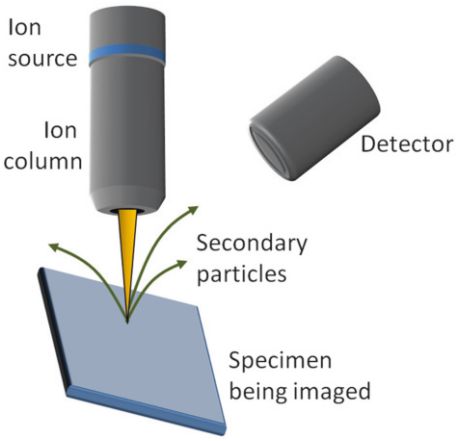

Fig. 7.2 Diagram of the helium ion microscope showing the ion source, the ion column, the sample, the detectable particles, and the detector

development [3]. A simplified diagram of the HIM is shown in Fig. 7.2. The helium ion source produces an ion beam with a typical energy of 30 keV and an ion beam current of about 100 pA. The beam enters the ion column, which includes steering deflectors, apertures, stigmators, scanning deflectors, and focusing elements. As the beam exits the column, it is focused to a very small probe size on the surface of the specimen. Typically, this probe size is 0.5 nm although measurements as small as 0.21 nm have been attained. The specimen can be virtually any shape or size, and a mechanical stage allows the sample to be reoriented to provide alternative perspectives. The entire beam path and specimen are maintained under a vacuum of better than 2×10^{-7} Torr.

As the focused beam strikes the sample at a particular location, it produces a number of particles that can subsequently be detected. The properties of the generated particles (their abundance, energy, angle, etc.) reveal some property about that particular location. The beam is then advanced to a new location (perhaps just 1 nm away), and the emitted particles are again detected. The variation in the quantity or properties of the generated particles provides the contrast from location to location on the sample. The focused helium beam is advanced in a raster pattern across a rectangular region of the sample (as shown in Fig. 7.2). The image is then assembled on a pixel-by-pixel basis as the beam is advanced. The gray level of each pixel is based upon a chosen property of these generated particles. For example, the pixel may be assigned black if there are no secondary electrons produced, or white if 10 or more secondary electrons are produced at that location. The typical time to acquire such an image can vary from 5 s to 5 min, depending on the signal-to-noise ratio required and the number of pixels in the final image (Fig. 7.3).

In some respects, the HIM operates much like the traditional SEM or gallium focused ion beam (FIB). In these regards, there are excellent textbooks that detail

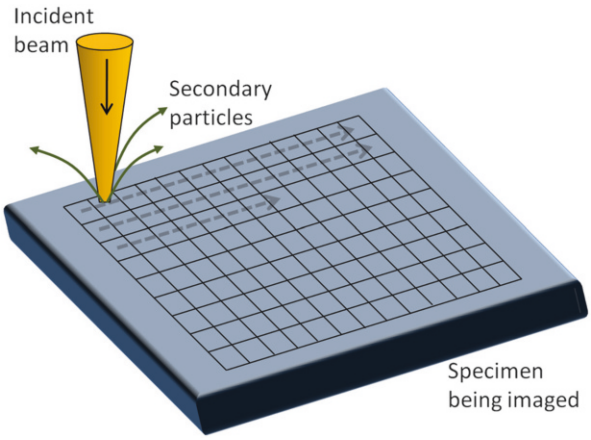

Fig. 7.3 The focused helium beam is moved from location to location in a raster pattern across the sample. Each of the locations on the sample corresponds to a pixel in the final image. Each pixel is assigned a gray level based upon the generated particles at the corresponding position

the basic physics that is common to their operation [4]. However, in many important ways the technology of the HIM is distinctly different. Only the most significant of these differences are therefore detailed in the following sections.

7.2.2 The Helium Ion Source

The helium ion source [5] is the key enabling technology for the HIM. A fuller description of the technology can be found in the established literature [6], but a cursory description is provided here. The ion source consists of a needle that is drawn to an atomically sharp end form (Fig. 7.4). The ion source operates at a temperature of about 70 K, in an ultrahigh-vacuum (UHV) vessel, with a large positive voltage applied to it. The apex of this tip has an underlying spherical shape (radius ~1,000 Å). Superimposed on this spherical shape is a three-sided pyramid terminating in an atomically sharp vertex. At this vertex, the single most protruding atom experiences an electric field, which can be as large as 4 V/Å. In this otherwise UHV region, ultrapure helium gas is admitted (impurity concentrations are typically 1 part in 10^6). Although neutral, the helium atoms become polarized and are drawn in toward the tip in the presence of the field gradient. This effect creates a region of elevated pressure surrounding the apex. The helium atoms are cooled by the process of repeated collisions with the cryogenic tip and eventually come to thermal equilibrium with the tip. As the low-energy helium gas atoms pass in the vicinity of the most protruding atom, the large electric field can cause a single electron to quantum mechanically tunnel [7] out of the helium atom and into the emitter tip. The remaining positive helium ion is now repelled by the positively biased tip and is

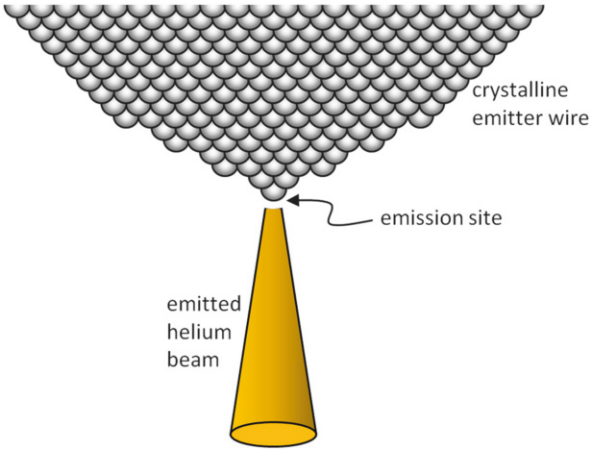

Fig. 7.4 The helium ion source produces helium ions originating from an atomically sharp asperity at the end of a positively biased needle maintained at cryogenic temperatures

immediately accelerated away. The field ionization process, which is key to this new microscope, was discovered over 50 years ago in the context of the field ion microscope (FIM) [8, 9].

Several unique properties of this ion source make it so desirable for high-resolution microscopy. First, the generated ions are produced from a region of atomic dimensions, and the virtual source size (established from back-tracking the ion's final trajectories) is less than 1 Å in size. Second, the beam diverges very gradually, with a typical emission cone semiangle less than 1°. Together, these two properties are reflected in the very high "brightness" of the ion source – routinely measured to be 4×10^9 A cm^{-2} sr^{-1} for a 25 keV beam [10]. Another important attribute is the monochromatic character of the ions. The energy spread, ΔE, of the beam is found to be about 1 eV or less, representing less than 1 part in 10^4 of the beam energy [11]. The low-energy spread is important to minimize the energy-dispersive effects as the beam is shaped and steered with electrostatic lenses and deflectors.

The usage of helium ions – as opposed to lighter- or heavier-charged particles – is ideal for imaging applications and offers advantages over the competing technologies of electron and gallium ion beams. The mass of an electron is so small that its wavelike properties begin to manifest themselves as the electron beam is focused. In fact, a highly optimized SEM will have its probe size significantly limited by diffraction [12]. For the helium ion beam, the de Broglie wavelength can be as small as 100 fm – not significantly affecting the focused probe size. Compared to gallium, helium is light enough that it does not cause excessive damage to the sample. In contrast, the massive gallium atom (atomic weight ~ 69 amu) is very effective [13] in sputtering away any specimen in which it strikes. Helium is also optically transparent, is chemically inert, and can diffuse out of biological specimens in relatively short times. For these reasons, helium is a convenient ion species for a charged

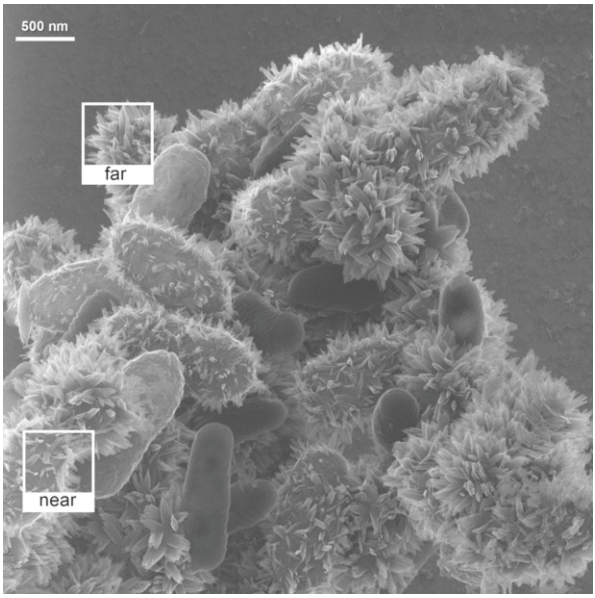

Fig. 7.5 A larger field of view of the same specimen shown in Fig. 7.1. This image shows that the sharpness is uniform throughout the image for both near (*lower boxed region*) and far features (*upper boxed region*). These are separated by an estimated 2 μm in depth

particle microscope. It will be mentioned in later sections that the same technology can be made to work with the heavier noble gas, neon. Such a neon beam offers a different type of sample interaction that can induce deliberate erosion of the specimen in a controlled manner with nanometer-level precision.

7.2.3 Probe Formation

After the ions are emitted from the ion source, they are accelerated into the optical column, which manipulates the beam to achieve the smallest attainable probe size on the sample. The beam is extracted from the ion source and emerges with an energy that varies from 15 to 45 keV. An electrostatic condenser lens is used to limit the rate of divergence of the helium beam. The column includes static deflectors for aiming the beam down the column and dynamic deflectors for scanning the beam in a raster pattern across the sample. An aperture is used to select only the central portion of the beam before it enters the final lens. Finally, the beam is focused with an electrostatic lens to achieve the smallest probe size at the surface of the sample.
As the beam is approaching the sample, it is roughly conical in its shape, with a convergence semiangle of less than 1 mrad. The small convergence angle also provides for a relatively long depth of field, making it easy to visualize samples with high aspect ratios (Fig. 7.5). The size of the imaged area (field of view) can span

from 100 nm to 1 mm, with as many as 2048 × 2048 pixels per image. The sample can be mounted to a standard stub or glass slide and be positioned anywhere from 4 to 40 mm below the final lens. Under optimal conditions, the helium ion beam can be focused to a probe size as small as 0.25 nm. Such images can resolve details otherwise not seen with an SEM or FIB. The sample can also be biased positively or negatively to enhance or diminish specific contrast mechanisms.

7.3 Beam–Specimen Interaction

As in an SEM or gallium FIB, the image generation in the HIM depends critically on how the particles comprising the focused beam interact with the specimen. Because the helium beam interaction is distinctly different compared to an SEM or a gallium FIB, the image contrast is distinctly different. The physics of the helium beam interaction is not fully understood, but several researchers [14–16] have begun unfolding the phenomena that underlie the images. These efforts will ultimately explain the mechanisms by which the HIM produces its high-contrast, high-resolution images. But even without our having a complete theoretical understanding of the contrast mechanisms, the HIM is establishing itself through the unique images it produces.

A basic understanding of beam–specimen interaction is best approached by considering the behaviors of individual helium ions incident upon the specimen. The fate of a single helium ion impinging upon a specimen can be understood from fundamental physics – primarily electrostatics and atomic-level scattering physics. In almost all circumstances, the incident particles do arrive one at a time, and their collision cascades are completed before the next particle arrives. The behavior of individual ions can then be combined by statistical methods to provide the average behavior of the helium ion beam. Such methodologies are commonly undertaken with Monte Carlo computer simulations. The remainder of this section relies heavily upon the IoniSE [16], TRIM [17], and Casino [18] computer programs to simulate the charged particles within the specimen.

7.3.1 Beam Penetration

A single helium ion interacts with the sample through a series of electrostatic interactions between the ion and the target nuclei and electrons that comprise the specimen. Most of these interactions produce small angular deflections whereby the trajectory of the helium ion is only slightly altered. These interactions tend to reduce the energy of the incident ion with a statistically averaged “stopping power” measured in energy loss per traveled path length (eV/Å). The stopping power determines how the particle is slowed down and eventually comes to a stop, and correspondingly how its energy is transferred to the specimen. The exact value of

Table 7.1 The stopping power for 25 keV helium ions into select materials

Specimen	Stopping power for 25-keV incident helium (eV/Å)
Water	6.1
Adipose tissue[a]	7.3
Cortical bone	9.7
Zinc	13.0
Osmium	14.8
Gold	16.0

[a]Berger MJ. Stopping powers and ranges for protons and alpha particles, International Commission on Radiation Units – Report ICRU-49. Bethesda, MD, USA: ICRU; 1993

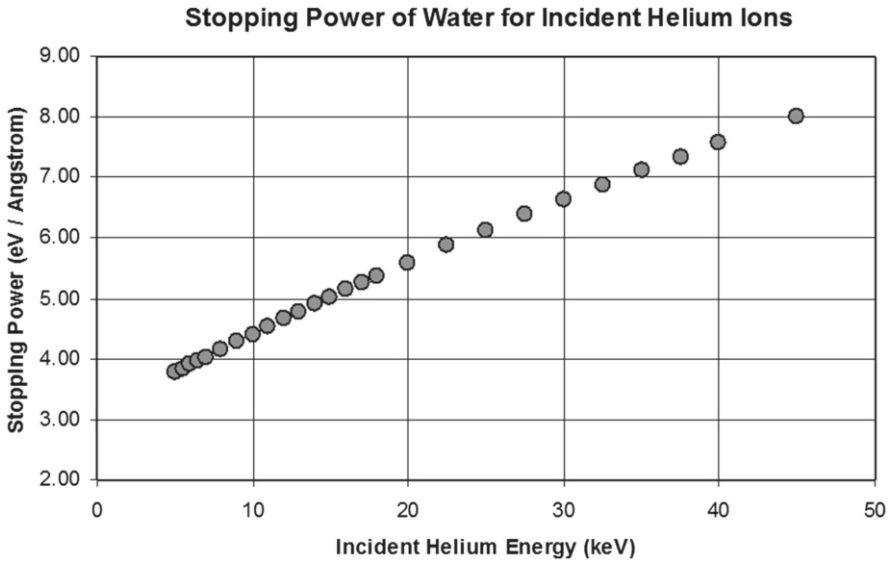

Fig. 7.6 The stopping power tends to decrease with decreasing energy

the stopping power depends on the composition of the specimen and the energy of the helium ion. The stopping power for 25 keV helium ions into select materials is shown in Table 7.1.

The stopping power tends to decrease with decreasing energy, as shown in Fig. 7.6. This energy is transferred from the helium ion to the electrons and nuclei of the specimen by several mechanisms. The relative importance of the different mechanisms may vary with beam energy and with the composition of the specimen, but the following estimates are valid for 25 keV helium into silicon: About 80 % of the energy transfer is to electrons – including ionization of the atoms in the specimen. These excited electrons are responsible for the production of secondary electrons – which will be discussed in the next section. The remaining 20 % of the energy is transferred to the nuclei of the sample, resulting in lattice vibrations (phonons), recoiled target atoms, and occasional backscattering events. As the

incident ion loses energy, the energy transfer to the nuclei tends to dominate over the energy transfer to the electrons. Ultimately, the stopping power is responsible for determining the average penetration depth of the helium beam.

As the helium ions penetrate into the surface of the specimen, there is a high probability that the helium ion will capture an electron within a few nanometers of the surface. Consider that helium is the most "electron-greedy" of all the residents of the periodic table. The helium ion will spend most of the rest of its trajectory (perhaps hundreds of nanometers) as a neutral helium atom. By this process of electron capture, the incident helium produces a very thin layer of positive surface charge over the top few nanometers of the surface. This is distinctly different from electrons, which are destined to keep their charge with them wherever they go – producing a deeper and widely distributed negative charging artifact. This simple difference is a distinct advantage for the HIM over the SEM and will be discussed in greater detail in a later section.

The helium ion's predominant interaction with electrons tends to produce a relatively small angular deflection of the incident ion, a consequence of the disparity in the masses: $M^{-}_{\mathrm{He}}/m_e \cong 7{,}300$. But there is a nonzero probability that the helium ion's trajectory will put it in line with the nucleus of a target atom. In this case, there is a strong electrostatic repulsion between the helium nucleus and the nucleus of the target atom. To some extent, these nuclei will be partly shielded by the remaining electrons. This resulting deflection is commonly known as Rutherford scattering [19]. In some cases, the helium atom is scattered backward out of the sample. These helium atoms are termed "backscattered," and their detection for the purposes of imaging is a subject addressed in the next sections. The probability of backscattering is typically 0.1 to 1 %, but this number increases for higher-atomic-number targets or for lower-incident-energy helium ions.

Due to the random nature of the collisions, the trajectories of the individual helium ions in the specimen vary considerably. Using the simulation software to simulate many thousands of ion trajectories reveals the general depth and shape of the interaction. From these simulations, it is also possible to determine the statistically averaged results, such as the average penetration depth and the average subsurface dispersion of the beam. The leftmost portion of Fig. 7.7 shows the general shape of the interaction volume for a 30 keV helium beam incident on a silicon specimen. The statistical nature of the scattering is evident in the varied trajectories (100 are shown here). Below the surface, the ions diverge in the shape of a well-defined cone (the typical cone angle is less than 5°) before broadening into a more spherical volume (not shown). The overall "teardrop" shape is common for many target materials and medium- to high-helium beam energies. In this particular case, the average incident helium beam penetrates to a depth of 350 nm. The shape of the interaction volume and the width near the surface are of critical importance for high-resolution-image formation – the topic of the next section. For comparison, the penetration of a 30 keV gallium beam is shown in the center of Fig. 7.7. For the more massive gallium beam, the nuclear scattering dominates, and the beam penetrates less deeply and broadens rapidly as it produces many displacements (shown as green dots) to the sample atoms. Surface sputtering is also quite significant for

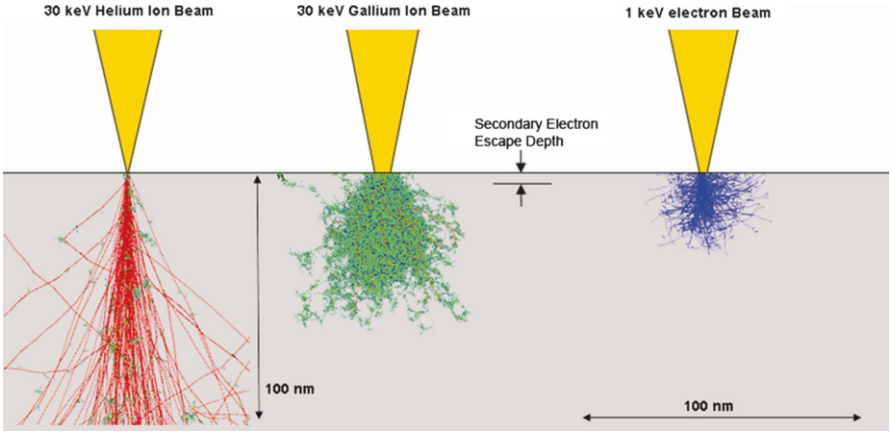

Fig. 7.7 Monte Carlo modeling results for representative beams into silicon. The *red* shows the trajectories of the incident particles (100 are shown for each case). The *green dots* indicate atoms of the specimen that have been displaced

such heavy ion beam species, causing the sample to be eroded as it is imaged. On the right of Fig. 7.7, a low-energy electron beam is shown for comparison. The electron beam interacts predominantly with the abundant electrons in the sample, and owing to their equal mass, they can scatter through large angles. Consequently, the beam disperses under the surface, and the interaction volume can be quite wide at the surface.

7.3.2 Generated Particles and Suitable Detectors

As the helium ion beam penetrates into the specimen, there are several particles that may be ejected from the specimen. The properties of these particles (including their abundance, charge, emission angle, or energy) can reveal information about the specimen that can vary from point to point (e.g., local topography or local composition). The detection of these particles, and their assumed variation from one location to another, form the basis for the contrast in the image. In the following section, the commonly encountered detected particles are discussed in detail.

7.3.2.1 Secondary Electrons

A secondary electron (SE) is any electron ejected from the surface with a kinetic energy below 50 eV. As with the SEM and gallium FIB, the SEs are the most commonly used detectable particle for image formation in the HIM. This is in part because of the relative abundance of SEs produced, and in part because of the

relative ease with which the SEs can be detected. Images that are based upon SE detection also reveal high-resolution and topographic information. The HIM has an advantage in producing many more SEs per incident particle (2 to 5) compared to the SEM, where the SE yield is typically less than 1.

As the helium ion enters the specimen, electrons are excited all along the ion's trajectory, but they can travel only a short distance (typically <3 nm) before their energy is dissipated. So it is only those electrons excited sufficiently close to the surface that may escape and be detected. Refer back to Fig. 7.7: The HIM has a unique advantage over the SEM or Gallium FIB in that the excited volume is quite narrow within the top few nanometers of the surface. Hence, the helium-induced SEs that can be detected will convey information about the intended location of the incident beam [20]. Compare this to the other beams, where the SEs can convey information that is less local because the near-surface excited volume is considerably wider. The result is a sharper image with the HIM.

The SEs that are generated from the incident beam as it first enters the sample are termed type-one secondary electrons, or "SE1," whereas if the SE is generated from the incident beam as it backscatters deeply and again passes near the surface, it is termed "SE2." Because of the relatively low backscatter yield of helium (~1 % for typical biomaterials), the SE signal consists almost entirely of SE1s and hence convey only surface information. For the electron beam, however, there is often considerable backscattering from deeper within the specimen, producing any number of SE2s as the incident electrons reemerges from the surface. The likelihood of the high angle scattering depends critically upon the subsurface composition, and hence the SEM's detector sees both surface and subsurface information conflated together [21].

The helium-induced SEs that escape the specimen typically have an energy [22] less than 2 eV. Due to their relatively low energy, their detection is relatively straightforward; they can easily be drawn toward any nearby electrode that is positively biased. The same technology used in the SEM, the Everhart–Thornley detector, has been adapted for usage in the helium ion microscope (Fig. 7.8). It consists of a highly transparent metal grid that is biased positively to about +500 V to attract the electrons. Once within the grid, the electrons are accelerated toward a scintillator that is biased to +10 kV. Upon striking the scintillator, a single electron will produce about 100 photons, which are optically guided down a light pipe and delivered to a photomultiplier tube (PMT). With a suitable gain, the PMT produces an easily measured electrical signal for each detected electron. The detection efficiency of such a detector depends critically upon the geometry of the sample relative to the detector grid and the final lens. The detection efficiency is commonly 80 %, but it tends to be reduced when the sample is very close to the final lens. A small positive bias can be applied to the sample to improve the performance of the detector.

The HIM images that are based upon the detection of SEs convey a detailed surface topography that is intuitively interpreted. The topographic information is evident in Fig. 7.9, which shows a complex three-dimensional arrangement of collagen fibers from a rabbit knee. Even to the untrained eye, each fiber's size, shape, banded texture, and three-dimensional arrangement are easily recognized. The visual cues that aid our interpretation include the characteristic bright-edge effect along the

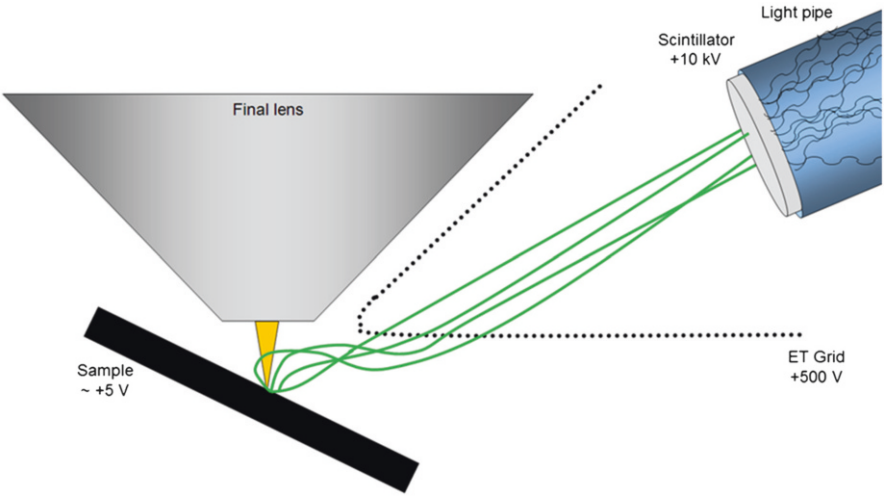

Fig. 7.8 A standard Everhart–Thornley detector is very effective in collecting secondary electrons and producing an electrical signal

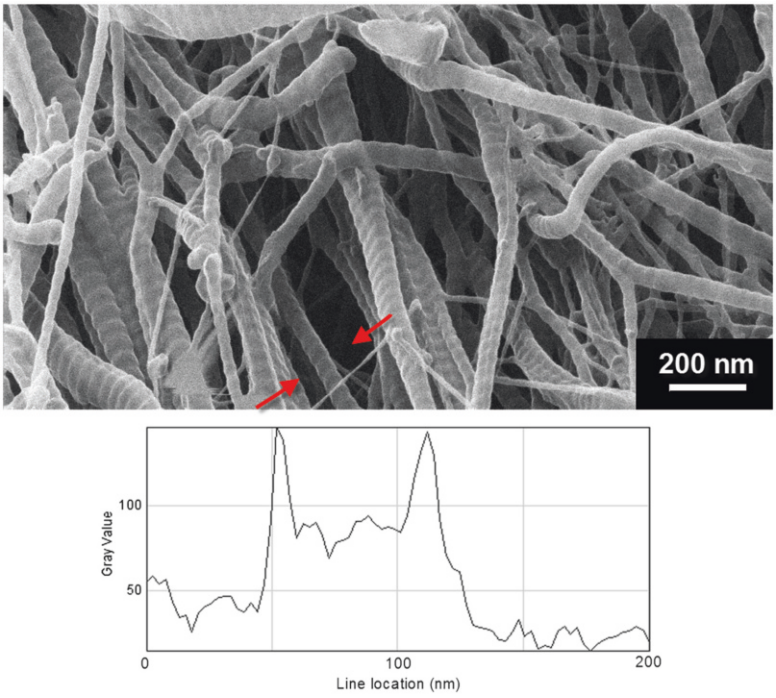

Fig. 7.9 The three-dimensional structure of collagen fibers is readily interpreted in this SE image from the HIM. Below the image, an individual line profile between the two *arrows* shows the bright edge effect (Sample provided by Wendy van den Berg-Foels, Clemson–Medical University of South Carolina Bioengineering Program)

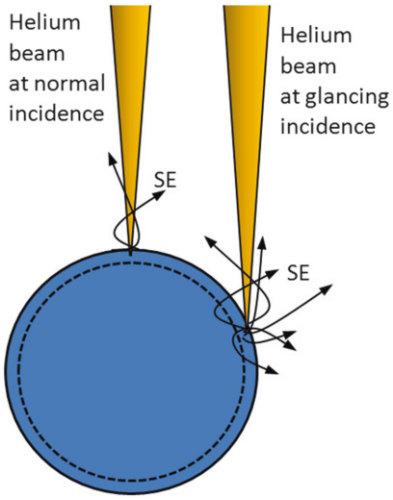

Fig. 7.10 As the helium beam enters the sample, electrons are excited all along its trajectory. When the beam enters at a glancing angle, more of these can escape and become detectable SEs, leading to a bright edge effect. The *dotted line* represents the characteristic escape depth of secondary electrons

edge of each fiber and can be explained as follows (Fig. 7.10): Where the beam strikes the sample at normal incidence, a small number (<5) of secondary electrons are produced, resulting in a darker gray pixel. In contrast, when the incident beam strikes the sample at a glancing angle, the beam remains close to the surface for a longer path length, and hence more SEs can escape and result in a brighter pixel. Experimentally, the bright-edge effect roughly corresponds to a brightness enhancement factor proportional to sec(α), where $\alpha = 0$ corresponds to the incident beam being parallel to the local surface normal.

Figure 7.9 also demonstrates the excellent depth of field afforded by the HIM. The more deeply situated collagen fibers are inherently darker because of the lower probability of SE detection – a visual cue that provides additional spatial information. Note also that the thinnest fibers are somewhat transparent: There are detectable SEs from the front surface as well as the back surface, as well as in further portions of the sample. This can lead to a transparency-like effect where the HIM conveys front surface information, superimposed on a more diffuse back surface information, superimposed upon a further portion of the sample.

7.3.2.2 Backscattered Helium

The small fraction of incident helium ions that undergo large angle scattering from the nuclei of the specimen can occasionally escape from the specimen and subsequently be detected. These backscattered helium ions may still be in the form of positive ions or they may be neutralized. The probability of backscattering is directly related to the scattering cross section, which in turn depends on the atomic number of the specimen atoms. According to the simple Rutherford scattering principles, the scattering probability should increase with the target atom's atomic number squared. Thus, an embedded gold nanoparticle would be more likely to produce a

backscatter event than the lighter elements found in biological specimens. Experimentally, this general trend is readily observed, but there are additional fluctuations that are not fully understood [23]. The unexplained fluctuations seem to correlate strongly with the group number (column number) of the periodic table, with copper, silver, and gold having scattering probabilities that are higher than most other elements in the same period (row).

The outcome of helium scattering can be most simply understood by considering the conservation of momentum and energy. Solving these equations yields the following equation [24]:

$$E_B = E_0 \left(\frac{\sqrt{M_2^2 - M_1^2 \sin^2 \theta} + M_1 \cos \theta}{M_1 + M_2} \right)^2 . \tag{7.1}$$

Here E_B is the energy of the helium atom just after the scattering, and E_0 is the energy just before the scattering. The masses of the incident helium ion and the target atom are M_1 and M_2, respectively. θ is the angle by which the helium atom's trajectory was changed (with 180° corresponding to a true backscatter). The simple physics is complicated by the fact that the helium atom loses energy through its many inelastic collisions throughout its trajectory (both before the scattering event and after).

In the ORION Plus instrument, the backscattered helium can be detected by two different methods. The first is a detector that produces a signal proportional to the abundance of detected backscattered helium. This is achieved with an annular microchannel plate (MCP) detector, which can be either retracted or inserted between the sample and the final lens, as shown in Fig. 7.11. When inserted, the MCP subtends a solid angle of about 1.8 sr. Because the backscatter rate is dependent on the atomic number, this detector provides a useful contrast to distinguish between heavy and light elements, with minimal topographic information. Because of the low rate of helium backscattering, this detector requires comparatively high exposures to generate images. The second option for detection of backscattered helium is a detector capable of simultaneously measuring the angle and energy of the individual backscattered helium atoms. This is achieved with a solid-state, energy-resolving detector with a limited acceptance angle. In the ORION Plus instrument, this detector has been used to identify unknown elemental composition or to determine the thickness of thin films [25].

7.3.2.3 Other Detectable Particles

In addition to secondary electrons and backscattered helium ions, photons have been observed to be emitted from some types of samples (Fig. 7.12). These have been measured with a simple PMT with a borosilicate glass window and a bi-alkali photocathode. Several materials have been tested, but only a small fraction of them seem to produce photons under the helium ion beam. The mechanism is not fully understood,

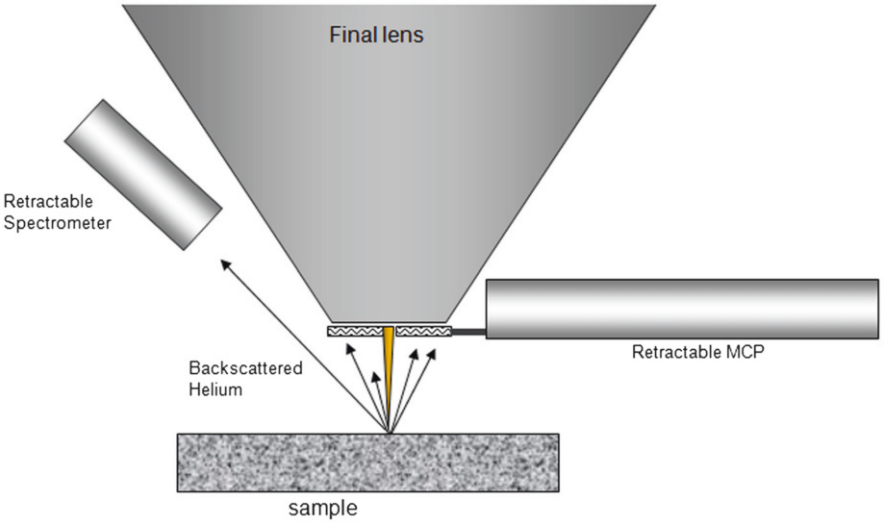

Fig. 7.11 The MCP detector can be inserted for use and provides an electrical signal for each helium atom (ion or neutral) that strikes it. Alternatively, the spectrometer can be used to analyze the angular and energy distributions

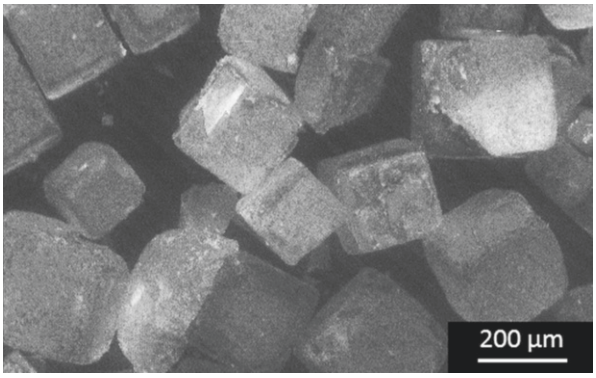

Fig. 7.12 The specimen is a collection of table salt. In this image, the grayscale was assigned based upon the abundance of detected photons

but two classes of mechanisms have been proposed. First, the photons can be the result of relaxation of the target atoms that have been raised to a higher energy state by action of the helium beam. This is akin to the cathodoluminescence (CL) effect, similar to what has been observed with SEMs. The spectrum of this emitted light could then be used to positively identify the target atoms by their emission spectra [26]. The other proposed explanation (which has no SEM counterpart) is that the photons are the result of the incident helium ions' returning to a lower energy state. This process will produce deep UV photons (~20 eV) as well as a broad range of visible and infrared photons.

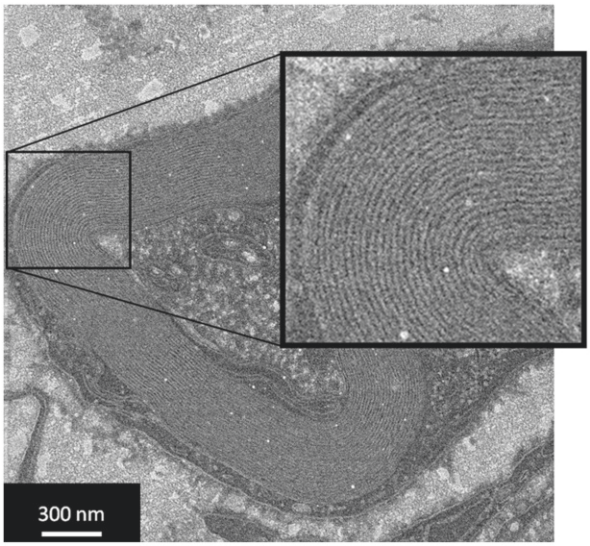

Fig. 7.13 Myelin sheets from a mouse cell as imaged with transmitted helium (Sample provided by Prof. Schroeder from MPI Heidelberg)

For either mechanism, the detection of these photons may reveal important information about the optical properties of the specimen in question. Recently, some HIM owners have equipped their systems with optical spectrometers for collecting and analyzing the photons that are produced [27]. Of special interest are the well-established fluorescent markers used in biomedical research.

Secondary ions and neutrals are known to be ejected from the sample when exposed to the focused helium beam. These are sputtered atoms from the sample and, as such, could provide useful imaging or analysis capabilities. A detector that can measure the gross abundance of all such secondary ions (SI) can provide an alternative imaging mode with a contrast that may be complementary to the SE contrast. Beyond this, one of several mass spectrometry techniques [28] can ascertain the atomic or molecular mass of the sputtered materials at the indicated location. Although a secondary ion mass spectrometer (SIMS) is not presently available for the HIM, there is ongoing work to develop such a commercially available detector for imaging and analysis [29]. Such an analysis technique could provide a mass resolution sensitive enough to distinguish different isotopes of the same element – enabling the use of isotopic markers.

Another type of detectable particle is the transmitted helium. For samples that are prethinned (typically 100 nm or less), the helium ions have a probability of passing through it with some angular deflection. The detection of the transmitted helium at a certain angle can provide a useful contrast mechanism that could complement the standard STEM imaging modes. An example of such an image is shown in Fig. 7.13. The image shows the myelin sheets from a mouse cell after it had been prepared by microtome and imaged in the ORION HIM with a transmission

detector. In this case, the detector was configured for "brightfield mode," collecting transmitted helium ions that suffered minimal angular deflections.

Lastly, it should be pointed out that the HIM is a relatively new instrument, and so there may be other particles that may be produced and may be detectable but have not yet been investigated. As we do with other new imaging technologies (i.e., the SEM in the 1950s), we anticipate the development of new detectors and new imaging modes as the instrument gains wider usage.

7.4 Sample Charging and Sample Preparation

Imaging biological specimens in the SEM requires several preparatory techniques to stabilize the materials to tolerate vacuum, to provide adequate contrast, and to minimize charging artifacts. While these preparations have been well established [30], they are known to introduce artifacts [31]. These artifacts are tolerable for some applications, but under highest magnifications, the sub 10 nm details reveal many distortions compared to the native state. In particular, the metallization of insulating samples with platinum or carbon will destroy or at least obscure the finer details. Operation of the SEM under high gas pressures (e.g., the environmental SEM) is one alternative to metal coating, but again there are resolution disadvantages that hide the sub 10 nm details.

Imaging with the helium ion microscope offers a unique advantage relative to the SEM in minimizing charging artifacts when imaging insulating samples or samples mounted to glass substrates. The first advantage is simply a result of the lower currents used in the HIM (1 pA typically) compared to the SEM (10 pA or more). A more significant difference between the HIM and SEM is in the distribution of the positive or negative charge. As mentioned earlier, the helium ions arrive in a single ionized state, and as they enter the specimen, they are apt to become neutralized and statistically spend most of the rest of their trajectory in a neutral state. Thus, beneath the surface, there is no net charge transport with the helium beam. In contrast, the electrons are deposited under the surface, where a negative space charge will accumulate. At the surface there is a relatively minor difference between the HIM and the SEM. The helium beam will produce positive surface charging because of two reasons: (1) the neutralization of the incident helium, and (2) the ejection of secondary electrons from the top few nanometers of the surface. The incident electron beam will also produce a positive surface charge, but only because of the ejection of secondary electrons from the surface. The effect is that the HIM produces only surface charging, and it is always positive in sign, whereas the electron beam induces positive surface charging *in combination with* negative subsurface charging. The net charging for the SEM can be either positive or negative depending on the relative contribution of these two effects. But even if they are exactly balanced and there is no *net* charging, there is still an electric field established between the subsurface (negative) and surface (positive) charging. The HIM comes equipped with a low-energy electron flood gun that easily mitigates the HIM's positive surface charging. However, an electron flood

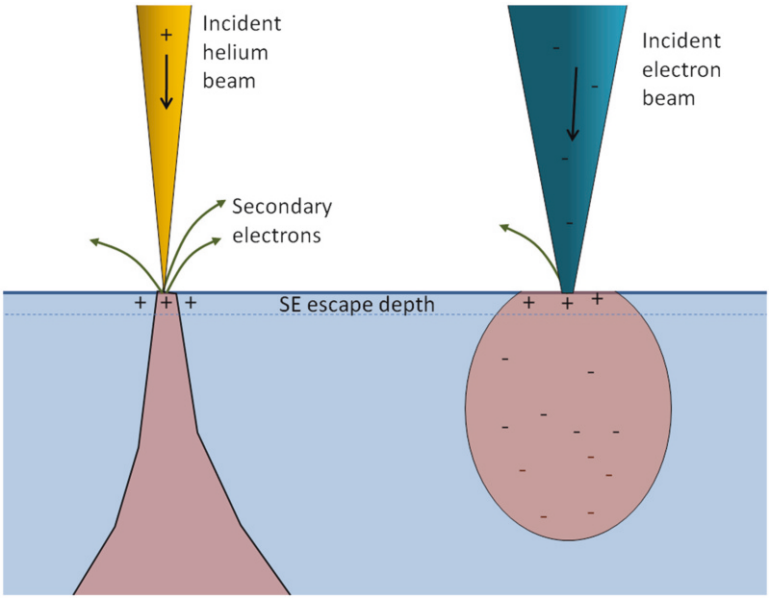

Fig. 7.14 The charging characteristics of the HIM (*left*) and the SEM (*right*). The HIM produces only positive surface charging within a few nanometers of the surface, which is easily mitigated with an electron flood gun. The SEM's subsurface charging has no known remedy

gun, or any surface treatment, cannot resolve both the surface and subsurface accumulated charge for the SEM. Figure 7.14 is a diagram comparing the charging situation for insulating samples from the HIM (left) and the SEM (right). For these reasons, the HIM has provided some exceptional imaging results on insulating samples that otherwise provide a challenge to image in the SEM.

An example of HIM imaging of an insulating sample is shown in Fig. 7.15. This image reveals the large-scale ultrastructure of mouse tooth enamel as imaged in the HIM without any special metal coating. Tooth enamel consists of extremely long and thin crystals of carbonated hydroxyapatite. The single crystals (70 nm wide and hundreds of microns long) are arranged in bundles (so-called enamel prisms) that are oriented in a species-specific and tooth-specific way to form a hierarchical structure that is very hard, but not brittle, and lends the tooth its mechanical properties (hardness and fracture resistance). The bundles represent former pathways of cells, controlling the growth of both the crystals and the bundles. The unique three-dimensional ultrastructure of the enamel represents a frozen map of the cell migration in the early development of the tooth. An SEM microscopist might have turned to a metallization technique in order to image this sample, but this would have compromised the fine detail and would likely have produced incomplete coverage due to the wildly varying topography.

The HIM's ability to image samples with minimal charging artifacts and with high resolution and contrast offers the microscopist a chance to image his or her samples

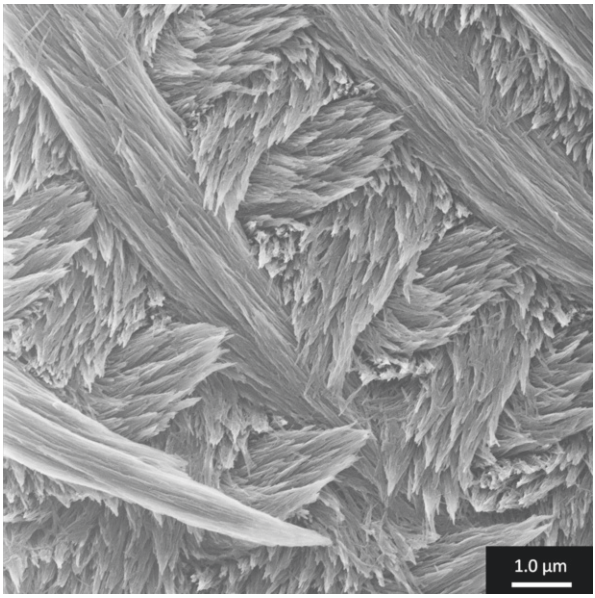

Fig. 7.15 Ultrastructure of mouse tooth enamel imaged without any metal coating in the helium ion microscope (Samples provided by Felicitas Bidlack of the Forsyth Institute, Cambridge, MA, USA)

with much less sample preparation. For highly three-dimensional structures, this avoids possible damage. Figure 7.16 shows a collecting duct of an intercalated renal cell. The collecting duct of the kidney absorbs water and nutrients out of the primary urine – an ultra filtrate of the blood. The intercalated cells play an important role in the acid–base homeostasis of the kidney. The intense membrane system of these cells bears H^+ ATPases regulating the pH of the primary urine. In the foreground (indicated by arrows), a primary cilium of the principle cells is visible. The exact function of this structure in the kidney remains unknown; one theory is that it has a role as a flow sensor in the collecting duct. HIM imaging of those structures reveals details that have not been observed before using conventional SEM.

The HIM offers the unique possibility to image biological samples with the without the necessity of conductive coatings. This capability, together with the extremely high resolution, can result in completely new insights on biological specimen. As with all microscopy techniques, improving resolution always unveils new and exciting details. It also means, though, that one enters the unknown with respect to what exactly can be observed and interpreted. Preparing a wet biological sample, fixing it, and drying it to make it vacuum-friendly inevitably changes the nature of the sample. If the sample is then imaged uncoated, it represents nothing but reality – or does it?

What happens if one can image without coatings in the sub 10 nm range is that sample preparation artifacts become obvious instantly. The difficulty one faces in omitting the well-known metal or carbon coatings is interpreting the results. Using the HIM on biological samples is rewarding in many aspects, and this chapter tries

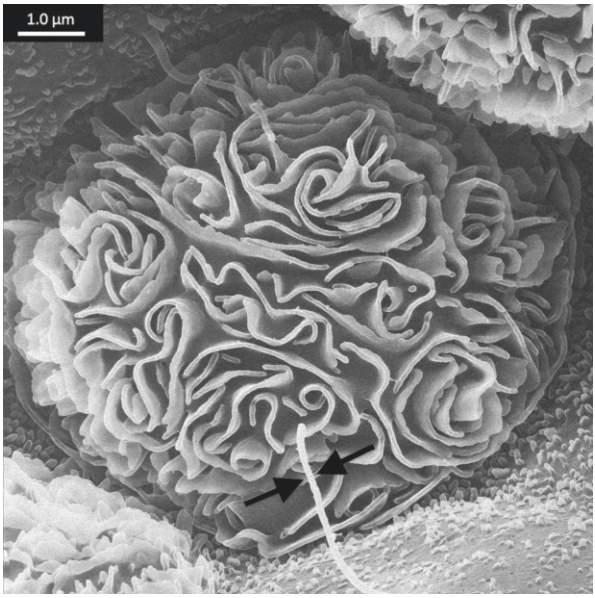

Fig. 7.16 The intercalated and principal cells of the kidney (Sample provided by Dennis Brown and Teodor Paunescu of Massachusetts General Hospital, Boston, MA, USA)

to convince the reader that it is worthwhile. It also means that the sometimes well-established sample preparation protocols for the SEM are a good starting point for HIM imaging but need to be modified for each sample type. The imaging of the collagen fiber network (Fig. 7.9) needed extensive optimization steps [32] in the preparation of the cartilage tissue. Figure 7.16 shows a rat kidney preparation that was possible only after a thorough development of a sample preparation protocol [33] for tissue samples. This protocol has been successfully adapted in the meantime for testis, retina, and inner ear samples (unpublished). In general, one has to be extremely careful not to damage the ultrastructure of the sample; what this involves is almost always very much dependent on what type of sample is under investigation. Once this hurdle is overcome, the results are very rewarding. Researchers are only starting to investigate their structures of interest using this new technology, and the results so far are very encouraging.

7.5 Future Outlook

The helium ion microscope remains a relatively new technology – much as the SEM was in the 1950s. Its strengths and weaknesses are still being recognized for biological and other application areas. New detectors and new methodologies are still evolving. Already mentioned was the prospect of generating images from the

detection of specific secondary ions, characteristic photons, and transmitted helium. Other nonimaging applications include manipulation of the specimen to support imaging. For example, recent work has demonstrated that this same technology can be extended to ion beam species other than helium. A focused neon beam, for example, has been generated with the same gas field ion source by changes to the emitter and the gas supply. The heavier mass of the neon atom will sputter away materials at a rate about 50 times faster than helium. Such a nanometer-sized focused neon beam can serve as a "nanoscale scalpel," able to remove material and expose hidden features that can be subsequently imaged. It is conceivable that three-dimensional information can be reconstructed through an alternating series of slicing and imaging procedures. In a recent publication by Joens et al. [1], the sheath of a predator nematoad was removed to expose the otherwise hidden tooth.

7.6 Summary

The newly developed helium ion microscope offers new imaging capabilities that are distinctly different from the traditional gallium focused ion beam or scanning electron microscope. The helium beam can be focused to a smaller probe size (as small as 0.25 nm) and can provide a greater depth of focus than the competing techniques. Most importantly, the helium beam interacts with the specimen in a distinctly different manner than electrons or heavier ions. The generated particles (including secondary electrons, backscattered helium, and others) provide rich contrast mechanisms that give information about the topography, composition, and other properties of the sample. For the imaging applications in biology, the HIM offers some unique advantages. In addition to the high resolution and long depth of focus, the helium beam can provide excellent contrast even on low-atomic-number materials such as carbon. The images that are produced from secondary electrons provide information that is specific to the top several nanometers of the sample. Most importantly, the HIM can provide imaging with a minimal sample preparations, allowing the researcher to have greater confidence that preparation artifacts are not occluding the features of interest. Also, insulating samples can be easily imaged at high magnification without the usual degradations and artifacts seen in the SEM.

References

1. Joens MS, Huynh C, Kasuboski JM, Ferranti D, Sigal YJ, Zeitvogel F, Obst M, Burkhardt CJ, Curran KP, Chalasani SH, Stern LA, Goetze B, Fitzpatrick JAJ. Helium ion microscopy (HIM) for the imaging of biological samples at sub-nanometer resolution. Sci Rep. 2013;3:3514.
2. Ward B, Notte J, Economou NP. Helium ion microscope: a new tool for nanoscale microscopy and metrology. J Vac Sci Technol B. 2006;24:2871–4.
3. Economou NP, Notte JA, Thompson WB. Scanning. 2012;34(2):83–9.

4. Goldstein J, Newbury DE, Joy DC, Lyman C, Echlin PE, Lifshin E, Sawyer L, Michael J. Scanning electron microscopy and X-ray microanalysis. 3rd ed. New York: Kluwer/Plenum Publishers; 2003. p. 49.
5. Tondare VN. Quest for a high brightness monochromatic noble gas ion source. J Vac Sci Technol A. 2005;23(6):1498–507.
6. Hill R, Notte JA, Scipioni L. In: Hawkes PW, editors. Advances in imaging and electron physics, vol. 170. Elsevier; 2013. p. 65–128.
7. Oppenheimer JR. Three notes on the quantum theory of aperiodic effects. Phys Rev. 1928;31:66–81.
8. Tsong TT. Atom probe field ion microscopy. New York: Cambridge University Press; 1990.
9. Müller EW, Tsong TT. Field ion microscopy, principles and applications. New York: Elsevier; 1969.
10. Hill R, Notte J, Ward B. The ALIS helium ion source and its application to high resolution microscopy. Phys Procedia. 2008;1:135–41.
11. Ernst N, Bozdech G, Schmidt H, Schmidt WA, Larkins GL. On the full-width-half-maximum of field ion energy distributions. Appl Surf Sci. 1993;67:111–17.
12. Reimer L. Scanning electron microscopy. 2nd ed. New York: Springer; 1998. p. 27.
13. Orloff J, Swanson LW, Utlaut M. Fundamental limits to imaging resolution for focused ion beams. J Vac Sci Technol B. 1996;14(6):3759–63.
14. Inai K, Ohya K, Ishitani T. Simulation study on image contrast and spatial resolution in helium ion microscope. J Electron Microsc. 2007;56:163–9.
15. Bell DC. Contrast mechanisms and image formation in helium ion microscopy. Microsc Microanal. 2011;17:147–53.
16. Ramachandra R, Griffin B, Joy DC. A model for secondary electron imaging in the helium ion microscope. Ultramicroscopy. 2009;109:748–57.
17. Ziegler JF, Biersack JP, Littmark U. The stopping and range of ions in solids, vol. 1, Stopping and ranges of ions in matter. New York: Pergamon Press; 1984. For the updated version, see SRIM Version 2013 (www.SRIM.com).
18. Drouin D, Couture AR, Joly D, Tastet X, Aimez V, Gauvin R. CASINO V2.42 – a fast and easy-to-use modeling tool for scanning electron microscopy and microanalysis users. Scanning. 2007;29(3):92–101.
19. Rutherford E, Geiger H, Marsden E. The scattering of α and β particles by matter and the structure of the atom. Phil Mag. 1911;Series 6, 21:669–88.
20. Sijbrandij S, Notte J, Sanford C, Hill R. Analysis of subsurface beam spread and its impact on the image resolution of the helium ion microscope. J Vac Sci Technol B. 2010;28(6):C6F6–9.
21. Goldstein J, Newbury DE, Joy DC, Lyman C, Echlin PE, Lifshin E, Sawyer L, Michael J. Scanning electron microscopy and X-ray microanalysis. 3rd ed. New York: Kluwer/Plenum Publishers; 2003.
22. Petrov YV, Vyvenko OF, Bondarenko AS. Scanning helium ion microscope: distribution of secondary electrons and ion channeling. J Surf Invest X-Ray Synchrotron Neutron Tech. 2010;4(5):792–5.
23. Kostinski S, Yao N. Rutherford backscattering oscillation in scanning helium ion microscopy. J Appl Phys. 2011;109:064311.
24. Rabalais JW. Principles and applications of ion scattering spectroscopy. Hoboken: Wiley Interscience; 2003.
25. Sijbrandij S, Notte J, Scipioni L, Huynh C, Sanford C. Analysis and metrology with a focused ion beam. J Vac Sci Technol B. 2010;28(1):73–7.
26. MacRae CM, Wilson NC. Luminescence database I – minerals and materials. Microsc Microanal. 2008;14(2):184–204.
27. Boden SA, Franklin TMW, Scipioni L, Bagnall DM, Rutt HN. Ionoluminescence in the helium ion microscope. Microsc Microanal. 2012;18(06):1253–62.
28. Benninghoven A, Rüdenauer FG, Werner HW. Secondary ion mass spectrometry: basic concepts, instrumental aspects, applications, and trends. New York: Wiley; 1987.

29. Wirtz T, Vanhove N, Pillatsch L, Dowsett D, Sijbrandij S, Notte J. Towards secondary ion mass spectrometry on the helium ion microscope: an experimental and simulation based study with He+ and Ne+ bombardment. Appl Phys Lett. 2012;101:041601.
30. Pawley J, Schatten H. Biological low-voltage scanning electron microscopy. New York: Springer; 2008.
31. Crang FE, Klomparens KL. Artifacts in biological electron microscopy. New York: Plenum Press; 1988.
32. Vanden Berg-Foels WS, Scipioni L, Huynh C, Wen X. Helium ion microscopy for high-resolution visualization of the articular cartilage collagen network. J Microsc. 2012;246(2):168–76.
33. Rice WL, Van Hoek AN, Păunescu TG, Huynh C, Goetze B, Singh B, Scipioni L, Stern LA, Brown D. High resolution helium ion scanning microscopy of the rat kidney. PLoS One. 2013;8(3):e57501.